Intermolecular Toroidal Conjugation: Circularly Stacked 16 π-Planes Formed by Supramolecular Assembly Enabling Cyclic Charge and Energy Delocalization

Daisuke Sakamaki,[*a] *Koki Tsubono,*[a] *Minami Nakamura,*[a] *Daiki Shimizu,*[b] *Yasunori Matsui,*[c] *Hiroshi Ikeda,*[c] *Ko Furukawa,*[*d] *and Hideki Fujiwara*[*a]

[a] Department of Chemistry, Graduate School of Science, Osaka Metropolitan University, Sumiyoshi-ku, Osaka 558-8585 (Japan)

E-mail: sakamaki@omu.ac.jp, hfuji@omu.ac.jp

[b] Department of Synthetic Chemistry and Biological Chemistry, Graduate School of Engineering, Kyoto University, Nishikyo-ku, Kyoto 615-8510 (Japan)

[c] Department of Applied Chemistry, Graduate School of Engineering, Osaka Metropolitan University, Naka-ku, Sakai, Osaka 599-8531 (Japan)

[d] Center for Coordination of Research Facilities, Institute for Research Administration, Niigata University, Nishi-ku, Niigata 950-2181 (Japan)

†Supporting information for this article is available on the WWW under http:xxxx

CCDC 2408185 and 2408186 contain the supplementary crystallographic data for this paper. These data can be obtained free of charge from The Cambridge Crystallographic Data Centre via www.ccdc.cam.ac.uk/data_request/cif.

Keywords: toroidal conjugation • through-space interaction • azaacene • phthalocyanine • time-resolved electron spin resonance

ORCID

Daisuke Sakamaki	https://orcid.org/0000-0001-6503-1607
Daiki Shimizu	https://orcid.org/0000-0002-2053-3483
Hiroshi Ikeda	https://orcid.org/0000-0002-8161-2177
Yasunori Matsui	https://orcid.org/0000-0002-7719-0071
Ko Furukawa	https://orcid.org/0000-0001-7665-8296
Hideki Fujiwara	https://orcid.org/0000-0002-4287-1547

Abstract

Toroidal conjugation is a unique way of charge and exciton delocalization via through-space overlap among circularly stacked π-orbitals, but the examples have been limited to intramolecular phenomena where π-planes are arranged around a hub molecule. In this study, we extend this concept to intermolecular phenomena and demonstrate the first example of intermolecular toroidal conjugation in designed systems, in which a circular π-stacked array is formed by molecular self-assembly. X-ray single-crystal analysis unequivocally revealed a toroidal array of 16 π-planes formed by the supramolecular dimerization of phthalocyanines substituted with eight pillar-like diazapentacenes interdigitating their π-pillars. The experimentally determined interplanar distances in the toroidal π-stacking array were close enough to realize through-space conjugation. We investigated the existence of charge and exciton delocalization in the toroidal π-stacking array using various steady-state and time-resolved spectroscopies and found that the positive charge migrated in the toroidal π-stacking array in the cationic and photoexcited states.

Introduction

Electronic conjugation is one of the most important concepts in the field of chemistry owing to its relationship with a diverse range of chemical phenomena. The concept of electronic conjugation was originally developed to describe the delocalization of electrons in successive p-orbitals, that is, π-conjugation.[1] Its scope was later extended to much wider systems, including other types of orbitals, except for the delocalization among p-orbitals, such as σ-conjugation,[2,3] σ,π-conjugation,[4] and π,d-conjugation,[5,6]

and so forth. In addition to these electronic communications through chemical bonds, through-space orbital interactions are also important, particularly in relation to charge and energy transport phenomena.[7] In 2005, Kochi proposed a unique type of conjugation called toroidal conjugation,[8] in which through-space orbital interactions between cofacially stacked π-planes continue circularly; that is, a toroid of successive π–π interactions (Figure 1a). In the first report on toroidal conjugation, a hexaarylbenzene skeleton was used as a hub unit for a toroidal array composed of six π-planes (Figure 1b). They generated the radical cation of a hexaarylbenzene substituted with six electron-donating diethylamino groups (**A**) and concluded that the positive charge was delocalized over all six donor groups through spatial overlaps of the π orbitals of the carbon atoms attached to the central benzene ring.[8–10] Although the situation of toroidal conjugation is similar to the concept of σ-aromaticity observed in the dications of hexaiodobenene[11] or hexakis(phenylselenyl)benzene,[12] Kochi et al. distinguished them from the dimensionality of the interactions; the orbital overlap in σ-aromaticity is essentially circular, but that in toroidal conjugation has three-dimensional fashion owing to face-to-face overlap.[8,9] Prior to the proposal of the concept of toroidal conjugation, Warman and Meijer et al. studied the excited-state dynamics of hexacarbazolylbenzene (**B**) and concluded that excimer-like interactions between carbazole units rapidly migrated around the six-carbazole array (more than 1000 round trips within an excited-state lifetime of approximately 5 ns).[13]

The possibility of toroidal conjugation around enlarged scaffolds larger than a benzene ring, such as perarylated acenes or more flexible perarylated polyacetylenes, was mentioned in the first proposal of the concept of toroidal conjugation.[8] In 2019, Bäuerle

et al. reported the synthesis of deca(2-thienyl)biphenyl, in which through-space electronic interactions can occur among 10 thiophene units around the biphenyl core;[14] however, such examples are very limited. In addition, to the best of our knowledge, the concept of intermolecular toroidal conjugation, that is, toroidal conjugation in which a π-stack array is formed by the assembly of more than one molecule, has not yet been proposed. Intermolecular toroidal conjugation is an attractive target from the viewpoints of physical organic chemistry and supramolecular chemistry, as well as functional materials and biochemistry, because the light-harvesting antenna complex (LH2) from a purple photosynthetic bacterium contains a toroidal array composed of 18 bacteriochlorophyll *a* (Bchl *a*) molecules, which might be regarded as a natural example of intermolecular toroidal conjugation.[15,16] The development of design principles for artificial systems with intermolecular toroidal conjugation will lead to a deeper understanding of photosynthesis mechanisms and the emergence of novel applications.

In 2019, we reported the synthesis of phthalocyanines (Pcs) substituted with eight pillar-like π-units, 6,13-dihydro-6,13-diazapentacene (DHDAP) bearing a hexyl side chain (**1a**) (Figure 1c).[17] Compound **1a** possesses four pairs of cofacially stacked DHDAPs connected through an *ortho*-phenylene group and four voids between the pairs of DHDAP, and **1a** can form a dimeric associate $\mathbf{1a}_2$ by inserting pairs of pillars into the voids of the counterpart monomer. As the result of the interdigitation of π-pillars, $\mathbf{1a}_2$ is considered to possess a toroidal array composed of 16 DHDAP units. Interestingly, **1a** and $\mathbf{1a}_2$ were isolated as different chemical species, even though $\mathbf{1a}_2$ is a van der Waals complex, and both **1a** and $\mathbf{1a}_2$ do not interconvert in THF even at 333 K. In our first report, we investigated the structures of **1a** and $\mathbf{1a}_2$ using various NMR techniques and mass spectrometry, in addition to ESR measurements for Cu-analogues of **1a** and $\mathbf{1a}_2$.[17] We

also investigated the kinetics of the interconversion between **1a** and **1a**$_2$ by varying the temperature and hydrostatic pressure.[18] In the course of our research, we conceived the idea that the cyclic arrangement of the 16 DHDAP pillars on the periphery of **1a**$_2$ may be a platform for realizing intermolecular toroidal conjugation. However, we have not succeeded in the single-crystal X-ray analysis of **1a**$_2$ because of its low crystallinity. Visualization of the toroidal π-stacking array is essential for proving the concept of intermolecular conjugation; therefore, we aimed to confirm the structure of the dimeric associate unequivocally using single-crystal X-ray analysis by synthesizing an analogue with increased crystallinity. In this study, we report the first structural analysis of a designed intermolecular toroidal π-stacking system based on single-crystal X-ray analysis and demonstrate the existence of intermolecular toroidal conjugation, that is, the circular delocalization of the charge and exciton in supramolecular associates, using various spectroscopic methods in combination with theoretical calculations.

Results and discussion

Synthesis and structure analysis of toroidal π-stacking array

Based on the hypothesis that the low crystallinity of **1a**$_2$ is caused by the flexible *n*-hexyl side chains, we synthesized various analogues of **1a** with different side chains. As the introduction of shorter alkyl chains (methyl or *n*-propyl) decreased the solubility too low to yield good crystals, we synthesized ZnPc with phenethyl groups (–CH_2CH_2Ph) on DHDAP units (**1b**), expecting a balance between the solubility and intermolecular interactions. Similar to **1a** and **1a**$_2$, **1b** and **1b**$_2$ were interconvertible by heating in specific solvent (See the next section for details), and **1b** and **1b**$_2$ were isolated as different chemical species. Although the solubilities of **1b** and **1b**$_2$ were lower than those of **1a** and

1a$_2$, they were moderately soluble in THF, dichloromethane, and aromatic solvents. The ^{1}H NMR spectra of **1b** and **1b**$_2$ were consistent with those of **1a** and **1a**$_2$, except for the differences in the side chains, indicating that **1b**$_2$ had the same association mode as **1a**$_2$ (Figures S5 and S7). Dimeric associate **1b**$_2$ crystalized in the tetragonal space group *P*4/*n* with unit cell lengths of $a = b = 33.9544(3)$ Å and $c = 19.1808(3)$ Å by slow evaporation of the THF solution in saturated ethyl acetate vapor (Figure 2a). As expected from the NMR spectra, **1b**$_2$ has a crystallographically four-fold symmetric structure where the two **1b** molecules densely bound to each other. It was unambiguously determined that the pairs of DHDAP units of one monomer penetrated the voids between the pairs of DHDAP units of the other monomer. The Pc planes of each **1b** monomer are stacked cofacially, and the shortest intermonomer atomic contacts between Pcs are 3.25 Å. The space-filling model of **1b**$_2$ without ZnPcs (Figure 2b) clearly shows a toroidal array of 16 DHDAP units. A number of short contacts existed among the DHDAP units belonging to different monomers. As only two DHDAP units in each **1b** are crystallographically independent, there are two types of π-stacks between the DHDAP units belonging to different monomers, whose shortest atomic distances between the DHDAP units were 3.13 Å and 3.44 Å in the crystalline state. Because the inequivalence of the distances was thought to be averaged in solution, all DHDAP units can be in close proximity to their neighbors to realize through-space charge and energy transfer. The crystal structure suggested that the tightly interlocked structure maximized the contact area between the monomers and prevented their sliding motion, explaining the unusually high stability of **1a**$_2$ and **1b**$_2$ as van der Waals dimers. To visualize interactions in the dimeric associate, we performed the non-covalent interaction (NCI) analysis[19–21] based on the crystal structure of **1b**$_2$ (Figure 2c). Green surfaces, representing regions where van der Waals interactions exist,

were observed between the DHDAP units belonging to different monomers, clearly visualizing the existence of continuous π–π interactions in the toroidal array.

Steady-state spectroscopies and DFT calculations

UV–Vis–NIR absorption spectra of **1b** and **1b**$_2$ in THF were completely matched with those of **1a** and **1a**$_2$ in the wavelength region greater than 350 nm (Figure 3a). The Q-band of **1b**$_2$ (652 nm) was blue-shifted by 588 cm^{-1} compared to that of **1b** (675 nm), owing to the H-aggregation of two Pcs. Both **1a**$_2$ and **1b**$_2$ exhibited long-wavelength tails of up to 1200 nm, which were not observed for the monomers. The solvent dependencies of the interconversion behaviors of **1b** and **1b**$_2$ were the same as those of **1a** and **1a**$_2$. Both **1b** and **1b**$_2$ were not interconvertible in THF solutions. In ethyl acetate at 60 °C, **1b** gradually associated and was completely converted to **1b**$_2$ after 120 min (Figure S14). In *o*-dichlorobenzene at 50 °C, **1b**$_2$ gradually dissociated and was completely converted to **1b** after 120 min (Figure S15). In dichloromethane at room temperature, **1b**$_2$ dissociated very slowly and was converted to **1b** over one month (Figure S16).

DFT calculations were performed for the model compounds of the monomeric and dimeric species whose side chains were replaced with hydrogen atoms (**1c** and **1c**$_2$). In **1c**, the HOMO was distributed on the four pairs of DHDAP units, and the LUMO and LUMO+1 were doubly degenerate and localized on the Pc moiety (Figures 2b). In **1c**$_2$, the HOMO was delocalized over 16 DHDAP units, and cyclic overlaps of MOs among the DHDAP units were formed (Figures 2c). The LUMO and LUMO+1of **1c**$_2$ were also doubly degenerate and localized on the stacked Pcs, similar to **1c**. The HOMO of **1c**$_2$ was energetically higher than that of **1c** by 0.306 eV, suggesting that toroidal MO interactions of the 16 donor units elevate the HOMO level. The LUMO of **1c**$_2$ decreased from that of

1c by 0.244 eV, which could be attributed to the through-space interaction between the original LUMOs localized on the Pc planes. The highest 16 occupied MOs (HOMO to HOMO−15) of **1c**$_2$ were mainly composed of the original HOMOs of DHDAP, reflecting the higher electron donor property of DHDAP than Pc (Figure S24). The HOMO−16 was mainly distributed on stacked Pcs but was also distributed on the DHDAP moieties to a certain extent. From TD-DFT calculations, the lowest energy transition of **1c** was predicted at 681 nm with a large oscillator strength (f = 0.5007). In contrast, for **1c**$_2$, the lowest energy transition was predicted to be the NIR absorption at 1083 nm with a small oscillator strength (f = 0.0166). This lowest-energy excitation was composed of the following transitions: HOMO→LUMO and LUMO+1 (45%) and HOMO−16→LUMO and LUMO+1 (52%). Considering the distributions of these MOs, this excitation has a charge-transfer characteristic from the toroidal DHDAP array on the periphery to the central stacked Pc moiety.

To investigate the details of the non-covalent interactions in the associate, we performed energy decomposition analysis (EDA) for the optimized geometry of **1c**$_2$. EDA decomposes the interactions between two molecules into the following terms: electrostatic (ΔE_{ELEC}), dispersion (ΔE_{DISP}), Pauli repulsion (ΔE_{PAULI}), induced electron polarization (ΔE_{POL}), and charge transfer (ΔE_{CT}). Table 1 summarizes the results of EDA. The largest contribution to stabilizing the dimer was the dispersion interaction (ΔE_{DISP} = −1390 kJ mol^{-1}), and the electrostatic interaction was the second largest contributor (ΔE_{ELEC} = −1195 kJ mol^{-1}). The total stabilizing energy was 714 kJ mol^{-1}, which was nearly twice the covalent bonding energy of the C–C single bond (~400 kJ mol^{-1}), indicating that the interdigitated dimeric structure tremendously enhanced attractive

noncovalent interactions.

Spectroscopic studies for radical cation species

After that the toroidal π-stacking array has been successfully visualized, the greatest interest is whether the charge or energy can migrate in the toroidal π-stacking array. To answer this question, we performed various spectroscopic measurements of the monomeric and dimeric species in their neutral and oxidized states. To this end, we used **1a** and **1a**$_2$ with *n*-hexyl side chains, because of the limited solubility of **1b** in THF. First, we observed changes in the electronic absorption spectra of **1a** and **1a**$_2$ upon stepwise electrochemical oxidation in dichloromethane using an electrochemical cell (light pass length = 1 mm). Upon increasing the applied voltage, weak absorption bands in the NIR region below 8000 cm^{-1} (1250 nm) gradually appeared in both **1a** and **1a**$_2$, accompanied by some isosbestic points (Figures 4a and 4b and S17). These newly appeared NIR bands could be attributed to the radical cations of **1a** and **1a**$_2$. The NIR bands were observed more clearly for higher concentration solutions oxidized by 1 equiv. of tris(4-bromophenyl)aminium hexachloroantimonate (magic blue, MB)[22] per **1a** and **1a**$_2$ using a thicker cell (light pass length = 10 mm) (Figure S18). However, the peak tops of these NIR bands were outside the measurement range of this spectrometer (< 5000 cm^{-1}).

Therefore, we attempted to observe the whole structures of the NIR bands using an FT-IR spectrometer. Figure 4c shows the FT-IR spectra of dichloromethane solutions of **1a** and **1a**$_2$ oxidized with 1 equiv. of MB. As a reference, the radical cation of **2a**, which is the precursor of **1a,** was also measured. The NIR band of **2a**$^{\cdot+}$ exhibited its maximum at 3440 cm^{-1} (2900 nm). The NIR band of the cation of **1a** was broadened compared to that of **2a**$^{\cdot+}$, but its peak was located at approximately 4000 cm^{-1} (2500 nm) and did not

shift to a lower-energy region. In contrast, the peak of the cation of **1a**$_2$ exhibited significant low energy shift to approximately 2500 cm^{-1} (4000 nm). This low-energy shift aligns with the results for the radical cations of hexadonor **A** compared with bidonor and monodonor compounds.[8] The NIR band at approximately 2500 cm^{-1} was also observed for **1a**$_2$ oxidized with 2 equiv. of MB, but after the addition of 4 and 8 equiv., the lowest-energy bands were shifted to approximately 3300 cm^{-1}, which were close to that of **2a**$^{\cdot+}$ (Figure S19). These results suggest that the band at approximately 2500 cm^{-1} can be attributed to the charge-transfer band, where the positive charges and spins migrate in the toroidal π-stacking circuit of **1a**$_2$ in its mono- and dicationic species.

Next, we measured the ESR spectra of the radical cations of **1a** and **1a**$_2$ generated by chemical oxidation in dichloromethane. We used 0.2 equiv. of MB per **1a** and **1a**$_2$ as an oxidant to minimize the disproportionation. Both the radical cations of **1a** and **1a**$_2$ exhibited broad structureless ESR signals, but their *g*-values were different: 2.0038 for **1a**$^{\cdot+}$ and 2.0029 for **1a**$_2^{\cdot+}$ (Figure 4d). The *g*-value of **1a**$^{\cdot+}$ increased from that of **2a**$^{\cdot+}$ (g = 2.0028) and was larger than the typical values for organic radicals composed of C, H, and N, suggesting that a certain spin density existed on Zn. In contrast, the *g*-value of **1a**$_2^{\cdot+}$ was very close to that of **2a**$^{\cdot+}$, indicating that almost no spin density existed on Zn. The peak-to-peak widths (ΔH_{PP}) at 293 K were 5.4 and 4.8 G for **1a** and **1a**$_2$, respectively, which were significantly decreased form that of **2a**$^{\cdot+}$ (13.5 G). Because the ESR linewidth becomes narrower when the spin can be delocalized over multiple units compared to the radical localized on a single unit,[23] the spectral narrowing of **1a**$^{\cdot+}$ and **1a**$_2^{\cdot+}$ compared to **2a**$^{\cdot+}$ can be attributed to spin delocalization over multiple DHDAP units, and the spin in **1a**$_2$ is thought to be more delocalized than that in **1a**. Considering the larger *g*-value of **1a**$^{\cdot+}$ (2.0038) than that of **2a** (2.0028), the spin generated in **1a** is thought to migrate

among four pairs of DHDAP via the central ZnPc plane in a through-bond manner. In contrast, the similarity between the *g*-values of $\mathbf{1a_2}^{\cdot+}$ (2.0029) and that of **2a** strongly suggests that the spin generated in $\mathbf{1a_2}$ is hopping among the eight pairs of DHDAP in a through-space manner instead of passing through the central ZnPc planes. The linewidth of $\mathbf{1a_2}^{\cdot+}$ was narrower than that of $\mathbf{1a}^{\cdot+}$ at all measured temperatures (293–183 K), although the linewidths became broader with decreasing temperature, owing to the decrease in the rates of spin migration (Figure S20).

Time-resolved spectroscopies after photoexcitation

To investigate how the intermolecular toroidal π-stacking affects the excited-state dynamics, we performed two different time-resolved spectroscopies: transient absorption spectra (TAS) and time-resolved-ESR (TR-ESR) for **1a** and $\mathbf{1a_2}$. We measured the TAS using a nanosecond flash photolysis system for N_2-saturated THF solutions of **1a** and $\mathbf{1a_2}$ after irradiation with a laser pulse at room temperature. The excitation laser pulse was set to the Q-band of ZnPc (650 nm). For **1a**, no transient signal was observed after excitation (Figure S21), indicating that the excited state deactivated faster than the time-resolution limit of our experimental setup (< 20 ns). This result is consistent with the result that ZnPc substituted with eight carbazole units had excited-state lifetimes of ~ 5 ns.[24] In contrast, $\mathbf{1a_2}$ exhibited clear long-lived transient signals; a rising signal at 450 nm and a bleaching signal at 650 nm appeared after excitation (Figure 5a). The decay profiles of both signals were well fitted with single exponential functions with the lifetimes of 1.5 μs, indicating that these signals originated from the same excited species (Figure 5b). As the air-saturated solution of $\mathbf{1a_2}$ gave almost the same result, the observed signals could be attributed to the charge-separated (CS) state resulting from single-electron transfer from

the peripheral toroidal π-stacking circuit to the central ZnPcs, rather than the excited triplet species. The transient signal at 450 nm was close to the radical cation band of a dihexyl-substituted DHDAP at 446 nm (Figure S22). As the intensity of the Q-band of ZnPc decreases upon one-electron reduction to the radical anion species,[25,26] the observed bleaching at 650 nm could be attributed to the formation of radical anion species in the central ZnPc moiety. The reason why only **1a**$_2$ exhibited the long-lived TAS attributable to the CS state can be explained by the smaller HOMO–LUMO gap of **1a**$_2$ than that of **1a** or the elongation of the lifetime of the CS state in **1a**$_2$ owing to the charge delocalization of the positive charge in the toroidal π-stacking array.[13]

TR-ESR can detect excited triplet (T_1) states generated by intersystem crossing from the excited singlet state (S_1) and subsequent radical pairs of the CS states and provide crucial insights into them at the microscopic level.[27,28] Figures 6a and 6b show the TR-ESR spectra of the frozen solutions of **1a** and **1a**$_2$ in THF at 10 K. Suddenly after laser flash (t = 0.4 μs), both **1a** and **1a**$_2$ exhibited broad ESR spectra with fine structures stemming from the interaction between electron spins typical for triplet species (Figures 6c and 6d), which were well simulated using the spin Hamiltonian of the triplet states with the following ESR parameters: (D, E) = (710 MHz, 110 MHz) for **1a** and (310 MHz, 55 MHz) for **1a**$_2$. The D and E values for **1a** is consistent with that of the excited triplet state for the typical ZnPc.[29] The mean spin–spin distances r in the excited triplet states were calculated to be ~ 4.8 and ~ 6.3 Å for **1a** and **1a**$_2$, respectively. Considering that the radius of Pc is ~ 7 Å and that of the toroidal circuit is ~ 9 Å, the spins of the triplet species were thought to be located in the central Pc moiety for **1a** and in the stacked Pcs for **1a**$_2$. The triplet signal disappeared within 2 μs for **1a** and no signal was observed thereafter (Figures 6a and 6e). In contrast, for **1a**$_2$, the broad triplet signal changed to a narrow signal

approximately 1 μs after the excitation (Figures 6b and 6f). The lifetime of the narrow signal was much longer than the upper limit of the measurement timescale (t = 14 μs) (Figure S23). Considering the disappearance of the fine structure, the long-lived narrow signal is attributed to the spatially separated radical pair of the CS state generated by single-electron transfer from the peripheral DHDAP units to the central ZnPcs.[28,29] Similar to the results of TAS, only **1a**$_2$ exhibited the long-lived signals attributable to the CS state, and these results strongly suggest that the generated radical cation rotates in the toroidal π-stacked array, resulting in the longer lifetime of the CS state (Figure 6g).

Geometrical considerations of intermolecular toroidal systems

Finally, we discuss the necessary conditions for forming a toroidal π-stacking array by molecular assembly from a geometrical perspective. Considering that n π-planes are aligned in a circle perpendicularly to the circle with an interplanar distance of a, the radius of the circle r is represented as $r = a/(2\sin\frac{\pi}{n})$. The length a must be within an appropriate range in which π–π interactions among each π-plane become attractive rather than repulsive. If we consider the case of a toroidal array of 16 π-planes and the length a is set as 3.40 Å (sum of the van der Waals radii of the sp^2 carbons), the radius r is calculated to be 8.71 Å. This value is close to the average distance from the fourfold axis to the center of each DHDAP unit (9.3 Å) in the crystal structure of **1b**$_2$, indicating that Pcs have a suitable size as hub-molecules of toroidal arrays of 16 π-planes. Another important aspect is the X-shaped structure of Pc with four convex regions (benzo moieties) and four concave regions between them. Owing to this geometrical feature, the pairs of π-pillars of one Pc are well-accommodated in the concave regions of another Pc.

Because of the above two reasons, Pcs can be rationalized as unique scaffolds for constructing toroidal circuits composed of 16 π-planes. Geometrical considerations imply the possibility of constructing toroidal circuits using Pcs with π-pillars other than DHDAP and also provide a hint for realizing novel intermolecular toroidal circuits consisting of different numbers of π-pillars.

Conclusion

We demonstrated intermolecular toroidal conjugation in cyclic π-stacking arrays of 16 π-planes formed by supramolecular dimerization using phthalocyanines substituted with eight diazapentacenes. X-ray crystal analysis and theoretical calculations confirmed the structure of the toroidal π-stacking array of 16 π-planes and the toroidal through-space interactions among π-planes. Various steady-state and time-resolved spectroscopies revealed that the positive charges generated by oxidation or charge separation after photoexcitation migrated around the toroidal array via through-space interactions, and that the formation of the intermolecular toroidal array resulted in the long-lived charge-separated state. This study proves that Pcs are suitable platforms for constructing intermolecular toroidal arrays of 16 π-planes and provides a future design principle for other systems exhibiting intermolecular toroidal conjugation.

Conflicts of interest

There are no conflicts of interest to declare.

Acknowledgements

This work was supported by a Grant-in-Aid for Scientific Research (17H04874, 18K05264, 20H02726, JP21H04564, JP22H05377, JP24H01092, JP22K05069) from the Japan Society for the Promotion of Science (JSPS), a Grant-in-Aid for Transformative Research Areas (A) "Condensed Conjugation" (JSPS KAKENHI Grant Number JP20H05866, JP21H05494) from MEXT, Ogasawara Toshiaki Memorial Foundation, Shorai Foundation for Science and Technology, The Foundation for the Promotion of Ion Engineering, and Izumi Science and Technology Foundation. Computation time for the theoretical calculations was provided by Research Center for Computational Science, Okazaki, Japan.

Notes and references

[1] J. Thiele, *Justus Liebigs Ann. Chem.* **1899**, *306*, 87–142.

[2] M. J. S. Dewar, *Bull. Soc. Chim. Belg.* **1979**, *88*, 957–967.

[3] M. J. S. Dewar, *J. Am. Chem. Soc.* **1984**, *106*, 669–682.

[4] T. G. Traylor, H. J. Berwin, J. Jerkunica, M. L. Hall, *Pure Appl. Chem.* **1972**, *30*, 599–606.

[5] W. Suzuki, E. Fujiwara, A. Kobayashi, Y. Fujishiro, E. Nishibori, M. Takata, M. Sakata, H. Fujiwara, H. Kobayashi, *J. Am. Chem. Soc.* **2003**, *125*, 1486–1487.

[6] T. Kambe, R. Sakamoto, K. Hoshiko, K. Takada, M. Miyachi, J.-H. Ryu, S. Sasaki, J. Kim, K. Nakazato, M. Takata, H. Nishihara, *J. Am. Chem. Soc.* **2013**, *135*, 2462–2465.

[7] Li Jinshi, Shen Pingchuan, Zhao Zujin, Tang Ben Zhong, *CCS Chemistry* **2019**, *1*, 181–196.

[8] D. Sun, S. V. Rosokha, J. K. Kochi, *Angew. Chem. Int. Ed Engl.* **2005**, *44*, 5133–5136.

[9] C. Lambert, *Angew. Chem. Int. Ed Engl.* **2005**, *44*, 7337–7339.

[10] S. V. Rosokha, I. S. Neretin, D. Sun, J. K. Kochi, *J. Am. Chem. Soc.* **2006**, *128*, 9394–9407.

[11] D. J. Sagl, J. C. Martin, *J. Am. Chem. Soc.* **1988**, *110*, 5827–5833.

[12] S. Furukawa, M. Fujita, Y. Kanatomi, M. Minoura, M. Hatanaka, K. Morokuma, K. Ishimura, M. Saito, *Communications Chemistry* **2018**, *1*, 1–7.

[13] J. J. Piet, H. A. M. Biemans, J. M. Warman, E. W. Meijer, *Chem. Phys. Lett.* **1998**, *289*, 13–18.

[14] T. D. Leitner, Y. Gmeinder, F. Röhricht, R. Herges, E. Mena-Osteritz, P. Bäuerle, *European J. Org. Chem.* **2020**, *2020*, 285–294.

[15] G. McDermott, S. Prince, A. Freer, A. Hawthornthwaite-Lawless, M. Papiz, R. Cogdell, N. Isaacs, *Nature* **1995**, *374*, 517–521.

[16] M. Ketelaars, A. M. van Oijen, M. Matsushita, J. Köhler, J. Schmidt, T. J. Aartsma, *Biophys. J.* **2001**, *80*, 1591–1603.

[17] H. Saeki, D. Sakamaki, H. Fujiwara, S. Seki, *Chem. Sci.* **2019**, *10*, 8939–8945.

[18] T. Kinoshita, D. Sakamaki, G. Fukuhara, *ACS Omega* **2024**, *9*, 34719–34724.

[19] R. Boto, F. Peccati, R. Laplaza, C. Quan, A. Carbone, J.-P. Piquemal, Y. Maday, J. Contreras-García, *ChemRxiv* **2019**, DOI 10.26434/chemrxiv.9831536.v1.

[20] E. R. Johnson, S. Keinan, P. Mori-Sánchez, J. Contreras-García, A. J. Cohen, W. Yang, *J. Am. Chem. Soc.* **2010**, *132*, 6498–6506.

[21] J. Contreras-García, E. R. Johnson, S. Keinan, R. Chaudret, J.-P. Piquemal, D. N. Beratan, W. Yang, *J. Chem. Theory Comput.* **2011**, *7*, 625–632.

[22] N. G. Connelly, W. E. Geiger, *Chem. Rev.* **1996**, *96*, 877–910.

[23] J. R. Norris, R. A. Uphaus, H. L. Crespi, J. J. Katz, *Proc. Natl. Acad. Sci. U. S. A.* **1971**, *68*, 625–628.

[24] S. A. Majeed, B. Ghazal, D. E. Nevonen, P. C. Goff, D. A. Blank, V. N. Nemykin, S. Makhseed, *Inorg. Chem.* **2017**, *56*, 11640–11653.

[25] J. Mack, M. J. Stillman, *J. Am. Chem. Soc.* **1994**, *116*, 1292–1304.

[26] J. Mack, M. J. Stillman, *Inorg. Chem.* **1997**, *36*, 413–425.

[27] K. Furukawa, Y. Sugishima, H. Fujiwara, T. Nakamura, *Chem. Lett.* **2011**, *40*, 292–294.

[28] S. Jin, X. Ding, X. Feng, M. Supur, K. Furukawa, S. Takahashi, M. Addicoat, M. E. El-Khouly, T. Nakamura, S. Irle, S. Fukuzumi, A. Nagai, D. Jiang, *Angew. Chem. Int. Ed Engl.* **2013**, *52*, 2017–2021.

[29] L. Chen, K. Furukawa, J. Gao, A. Nagai, T. Nakamura, Y. Dong, D. Jiang, *J. Am. Chem. Soc.* **2014**, *136*, 9806–9809.

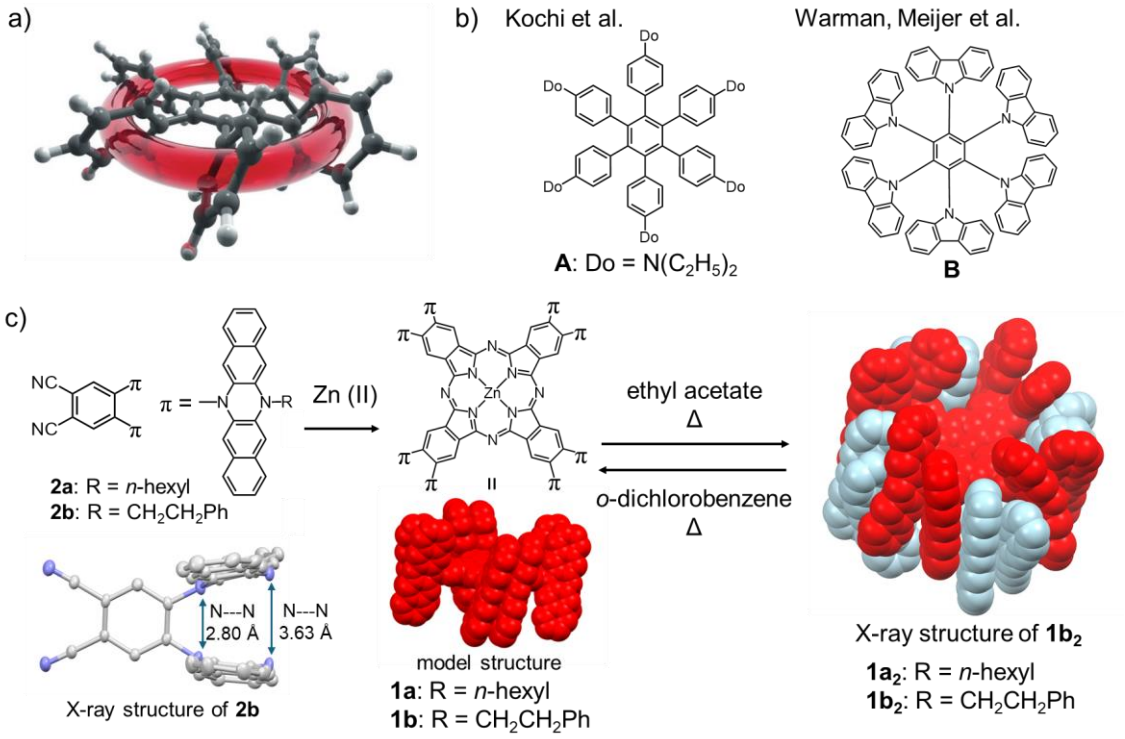

Figure 1. a) Schematic representation of toroidal delocalization of charge in hexaphenylbenzene radical cation. Reprinted with permission from ref. 9. Copyright 2005 Wiley-VCH. b) Examples of molecules exhibiting toroidal conjugation in their cationic or excited states. c) Synthesis of phthalocyanines forming toroidal π-stack array upon supramolecular dimerization. In crystal and model structures, side chains were omitted for clarity.

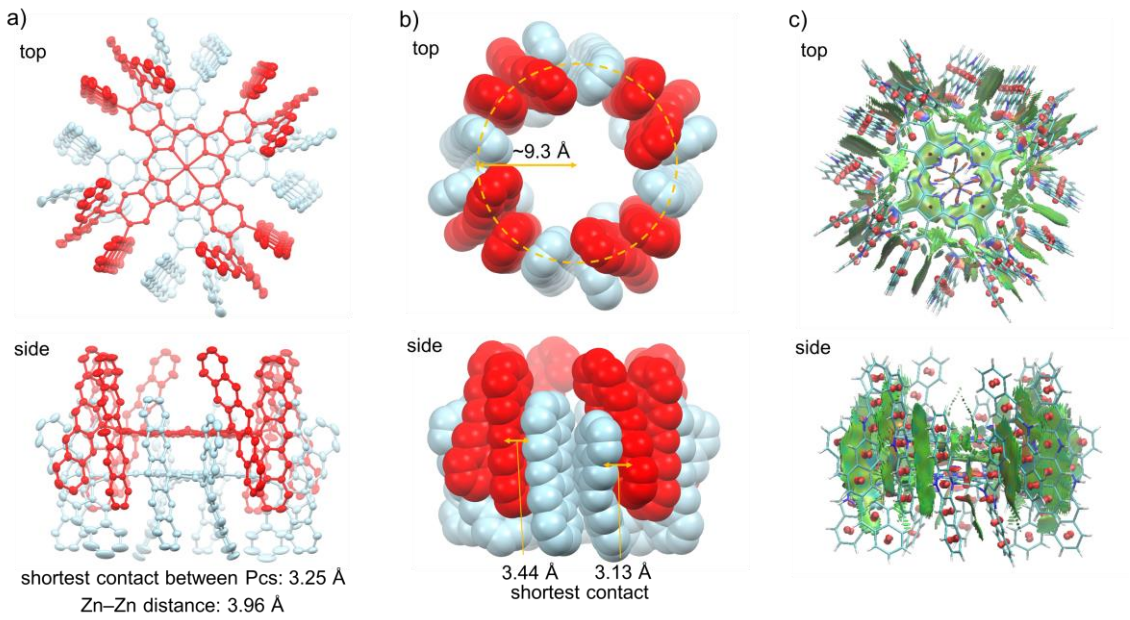

Figure 2. a) ORTEP representations of **1b**$_2$. Thermal ellipsoids are set at 50 % probability. b) CPK models of the toroidal π-stacking array composed of 16 DHDAP units in the crystal structure of **1b**$_2$. Phenethyl groups and hydrogen atoms were omitted in a) and b) for clarity. c) NCI plots for the crystal structure of **1b**$_2$. Phenethyl groups and Zn atoms were replaced by hydrogen atoms to reduce computational costs.

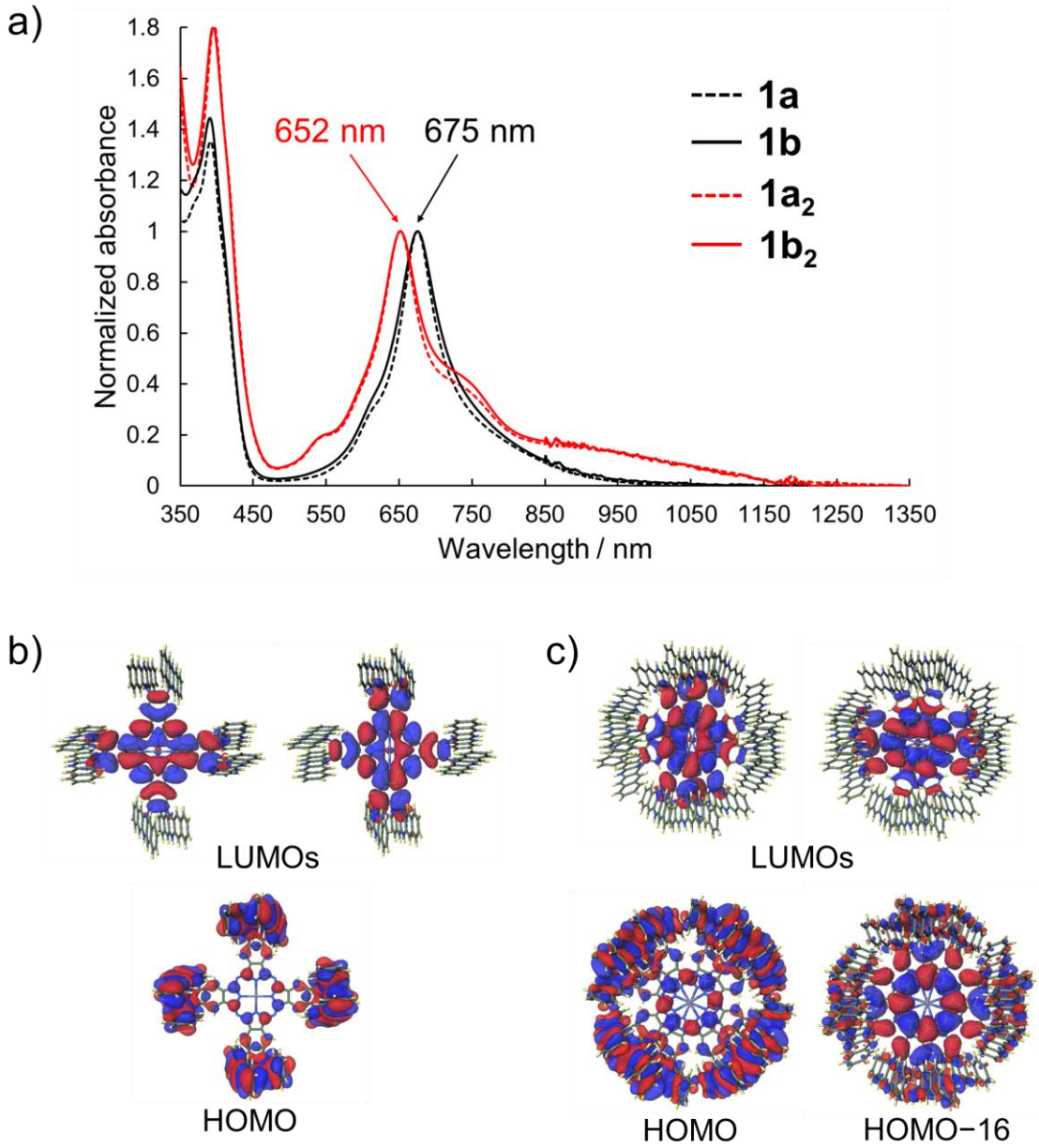

Figure 3. a) UV–Vis–NIR spectra of **1a**, **1b**, **1a**$_2$, and **1b**$_2$ in THF at room temperature. b) and c) Frontier MOs of model compounds **1c** and **1c**$_2$.

Table 1. Results of Energy decomposition analysis (second-generation ALMO-EDA) of **1c**$_2$ (kJ mol^{-1}) at the B3LYP-D3BJ/6-31+G(d,p) level of theory.

ΔE_{ELEC}	ΔE_{PAULI}	ΔE_{DISP}	ΔE_{POL}	ΔE_{CT}	Total
−1195	2068	−1390	−75	−121	−714

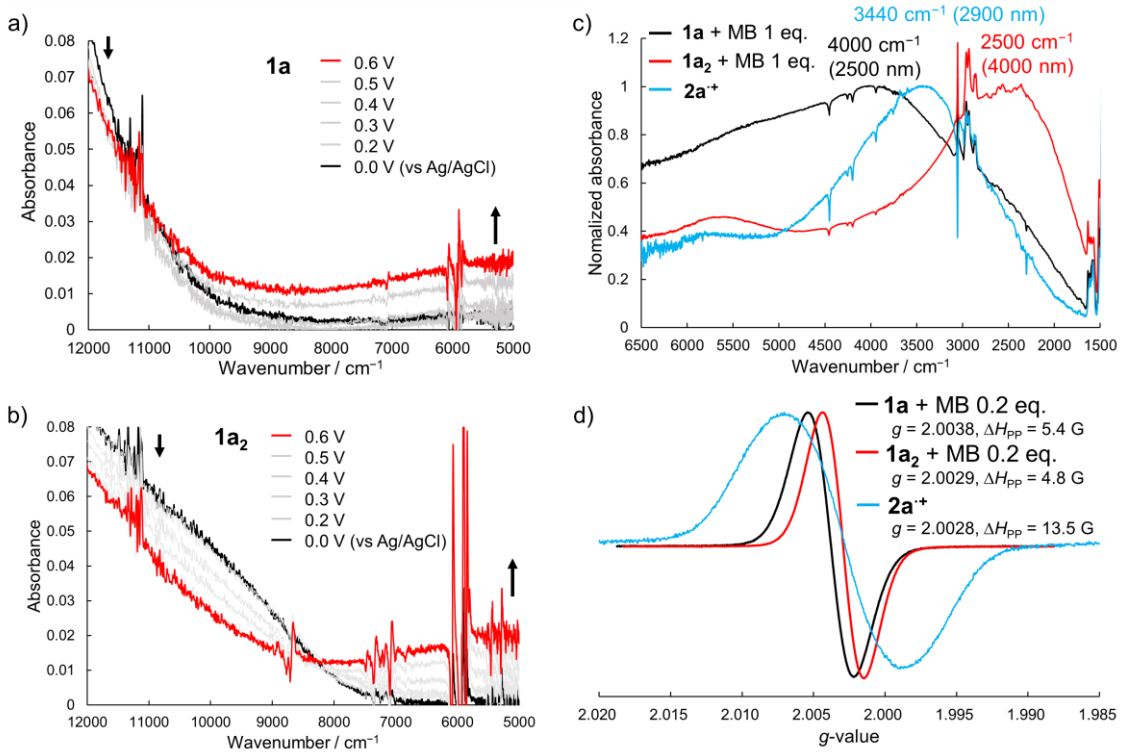

Figure 4. a) and b) Changes in NIR absorption spectra of **1a** and **1a**$_2$ during electrochemical oxidation from the neutral states (black lines) in dichloromethane containing 0.1 M *n*-Bu$_4$NBF$_4$. c) FTIR spectra of **1a** and **1a**$_2$ oxidized with 1 equiv. of MB and **2a**$^{\cdot+}$ in dichloromethane at room temperature. d) ESR spectra of **1a** and **1a**$_2$ oxidized with 0.2 equiv. of MB and **2a**$^{\cdot+}$ in dichloromethane at room temperature.

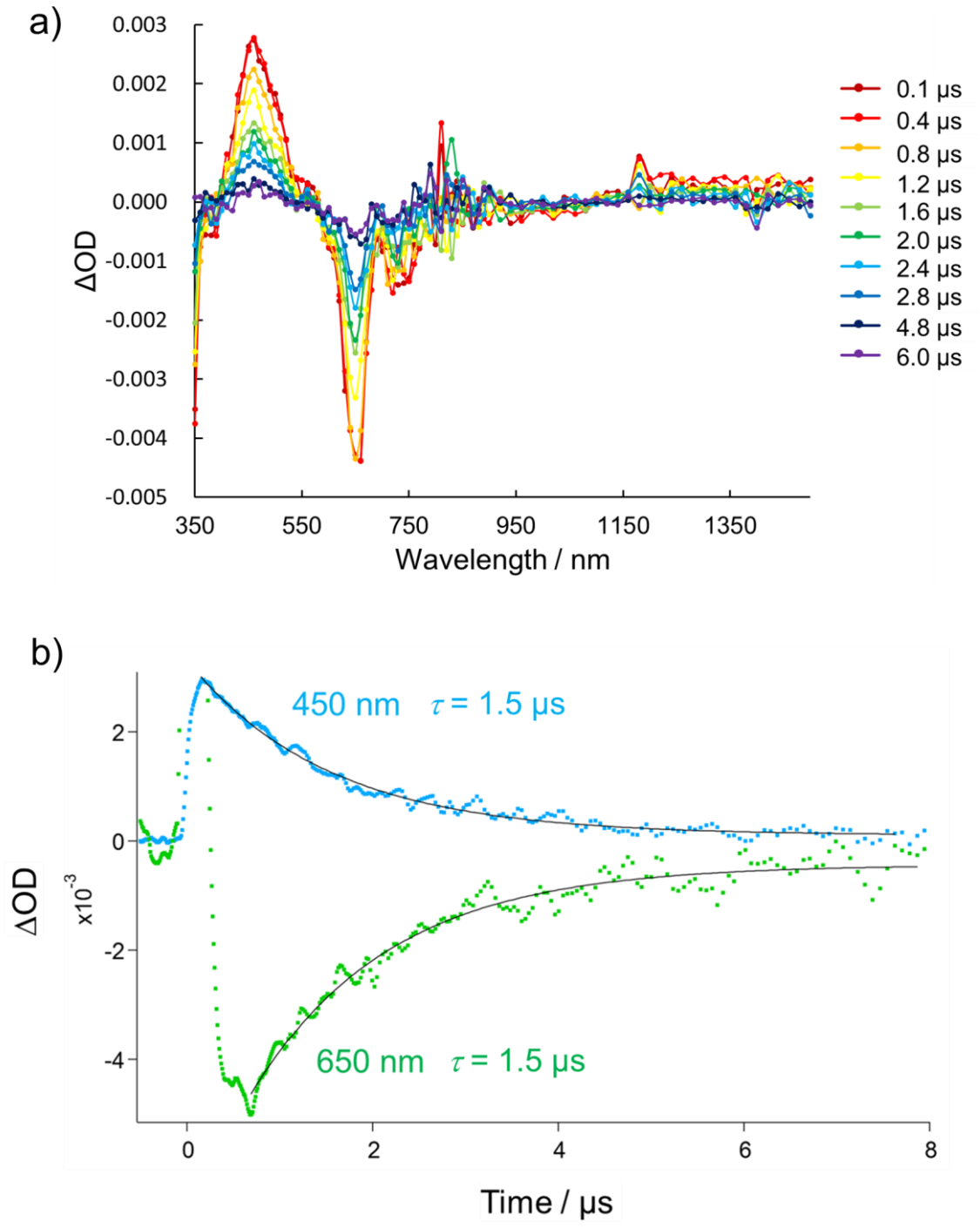

Figure 5. a) Transient absorption spectra of **1a**$_2$ in THF at room temperature (excitation wavelength = 650 nm) and b) kinetics at 450 nm and 650 nm.

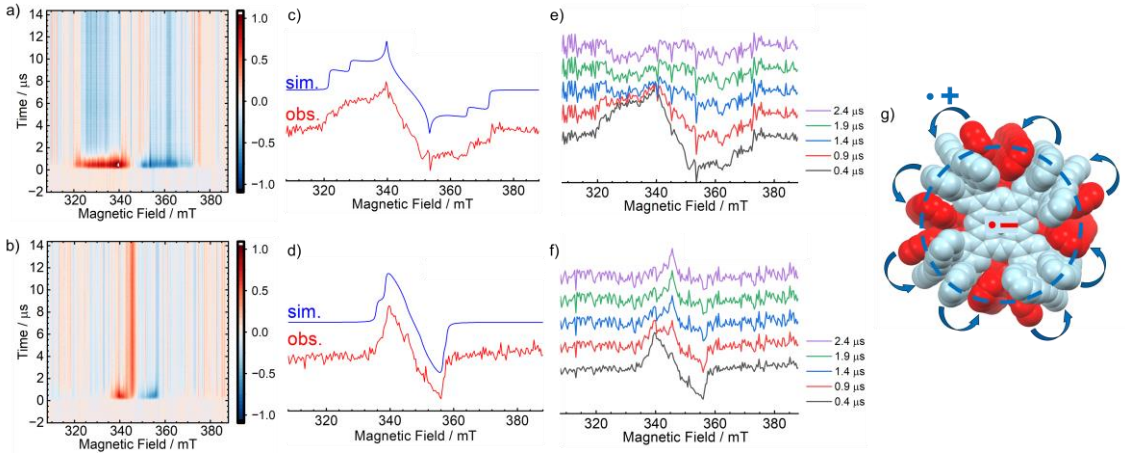

Figure 6. a) and b) 2D TR-ESR spectra for a) **1a** and b) **1a**$_2$ in THF at 10 K (excitation wavelength = 650 nm). The color scale denotes the signal intensity. Positive and negative values indicate the absorption and emission of microwaves, respectively. c) and d) Slice spectra along the magnetic field axis at t = 0.4 μs and their simulated spectra for c) **1a** and d) **1a**$_2$. e) and f) Temporal changes in 2D TR-ESR spectra for e) **1a** and f) **1a**$_2$. g) Schematic representation of the CS state of **1a**$_2$. Blue arrows indicate the intermonomer hopping of the hole site in the toroidal π-stacking array.